

See discussions, stats, and author profiles for this publication at: <https://www.researchgate.net/publication/272127840>

# Hot Injection Processes in Optically Excited States: Molecular Design for Optimized Photocapture

ARTICLE *in* THE JOURNAL OF PHYSICAL CHEMISTRY C · SEPTEMBER 2014

Impact Factor: 4.77 · DOI: 10.1021/jp5051172

---

READS

15

## 3 AUTHORS:



Gil Katz

Hebrew University of Jerusalem

38 PUBLICATIONS 419 CITATIONS

[SEE PROFILE](#)



Mark A. Ratner

Northwestern University

905 PUBLICATIONS 42,254 CITATIONS

[SEE PROFILE](#)



Ronnie Kosloff

Hebrew University of Jerusalem

440 PUBLICATIONS 15,465 CITATIONS

[SEE PROFILE](#)

# Hot Injection Processes in Optically Excited States: Molecular Design for Optimized Photocapture

Gil Katz\*,† Mark A. Ratner\*,‡ and Ronnie Kosloff\*,§

\*Afikim Science, Afikim Israel, Fritz Haber Research Center for Molecular Dynamics, Hebrew University of Jerusalem, Jerusalem 91904, Israel

†Department of Chemistry, Northwestern University, Evanston, Illinois 60208-3113, United States

§Institute of Chemistry and the Fritz Haber Research Center for Molecular Dynamics, Hebrew University of Jerusalem, Jerusalem 91904, Israel

## Supporting Information

**ABSTRACT:** Design principles for efficient solar photocapture using a single molecule are presented. The proposed molecular model is composed of ground and excited bright and dark electronic states. Once photoexcited to the bright states, vibrational relaxation and dissipation to the ground vibrational level of the bright state commonly occur. This degrades a substantial amount of the incoming photon energy into heat, further reducing the efficiency of molecular photocells. One way to circumvent this energy flow from electronic excitation into heat is the *hot injection* process, by which the original excited bright state undergoes a rapid crossing to an acceptor dark state, with a higher potential energy minimum, and is trapped in the region of that minimum. By choosing an appropriate pair of vibrational modes, the overall energy gain can be increased substantially and the constraints on the bath behavior substantially simplified. We present calculations in a two-dimensional vibrational space, along with energy relaxation and transfer to the bath (using a Stochastic Surrogate Hamiltonian model). We find that the second degree of vibrational freedom, if carefully chosen, strongly increases the efficiency and the possibility of successful hot injection. In addition, the same molecular model can be designed to utilize the red part of the solar spectrum. Excited state absorption can recycle the wasted bright state population thus increasing the efficiency of solar capture.



## INTRODUCTION

Solar energy harvesting is challenged by the broad energy spectrum of solar radiation spanning approximately  $\sim 2.5$  eV. Existing devices that convert the energy into charge carriers lose the low frequency end of the spectrum. This part has either photons that are lower in energy than the bright state or insufficient energy for generating charge upon photoexcitation. The high frequency end of the solar spectrum actually dissipates heat, which has to be removed. An engineering solution is to construct a multilayer device with each layer possessing a different band gap.<sup>1,2</sup> Another suggestion is to find nanomaterials where the high frequency end of the spectrum generates multiple charge carriers.<sup>3</sup> Here we propose a scheme where a single dye molecule can be designed to serve as a multilevel absorber, capturing the energy of a significant part of the solar spectrum energy.

Dynamics of photoexcited molecules, following Franck–Condon vertical excitation to a bright state, occur on multiple time scales; these include vibrational relaxation to the lowest vibrational level in the hot electronic state, which was believed to be a dominant dynamical process, which could occur before intersystem crossings, fluorescence, or nonradiative decay. This generalization (that subsequent dynamics occurs from the vibrational minimum of the bright state) is known as Vavilov's Law<sup>4–7</sup> and was an accepted assumption until the 1960s, when deeper understandings were gained about the actual time scales for dynamics in photoexcited manifolds. The Jablonski diagram

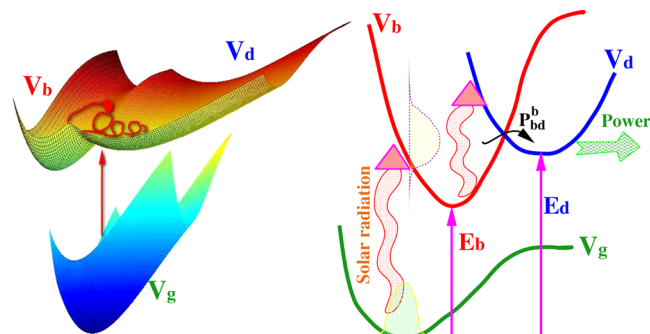


**Figure 1.** Three diabatic potential energy surfaces: the ground  $\hat{V}_g$ , bright  $\hat{V}_b$ , and dark  $\hat{V}_d$  potentials. On the right, a schematic one-dimensional cut in the potentials.

of Figure 1 shows that the amount of energy lost from the vertical excitation to the vibrational minimum of the bright state, termed  $\Delta E_B$ , can be quite large. This suggests that if it were possible to undergo an essentially irreversible electronic transition to a dark state before vibrational relaxation to the bright state minimum occurs the energy  $\Delta E_B$  in the Vavilov's Law regime is simply dissipated into the environment and can be

Received: May 24, 2014

Revised: August 26, 2014

Published: August 29, 2014



effectively captured into an electronic excitation. This is the idea of *hot injection*, originally introduced to describe systems composed of quantum dot components.<sup>8,9</sup>

Clearly, hot injection (HI) can be useful for increasing the efficiency of solar photovoltaics or solar fuels since substantial energy can be captured in the electronic dark state.

Previously,<sup>10</sup> we discussed this process for molecules with only one active vibrational degree of freedom. While that work described scenarios under which HI can occur and demonstrated that effective capture is indeed possible, the restriction to one dimension severely limits our ability to prevent recrossing, requiring some strong assumptions about decoherence times. Here, we generalize that analysis includes molecules with two or more active vibrational dimensions and show that the idea of HI is both more feasible and more straightforward in the multi-dimensional situation. This opens an opportunity for a new molecular design space, aimed at optimizing the utilization of the HI process in molecules. In addition, we incorporate the possibility of employing traditional solar absorption from the bright to the dark state, expanding the solar capture to the part of the red end of the spectrum.

To describe the appropriate dynamics, we need to consider a realistic situation, with dissipative processes both within the molecular entities and arising from the bath in which they are found. We need to formulate energy flows among all relevant levels, as well as dissipation into the bath. To do so, we utilize a multistate molecular Hamiltonian and a Stochastic Surrogate Hamiltonian (SSH) representation for the system/bath dynamics.<sup>10–12</sup> SSH replaces the bath degrees of freedom by a set of spin levels that constitute the primary bath and are coupled to a secondary bath which accepts energy (on a certain time scale) from the excited spin levels. SSH is flexible and efficient and allows (non-Markov) energy flow back from the primary bath into the system, a feature that may be important in realistic systems.

In our previous work,<sup>10</sup> the HI process was limited by the size of the vibrational manifold. Here we introduce a new concept: to separate the vibration storage mode from the dynamical (transfer) mode that describes surface crossings. One of these should be at high frequency and the others at low frequency. An example might be a system like a chemisorbed aldehyde on a surface like aluminum oxide. Dynamically, the first (molecular) vibrational mode is high frequency and describes the actual intersystem crossing to the dark state. The second (surface) mode's purpose is to absorb the excess energy and is generally a softer, more anharmonic vibration. By combining the vibrations in this manner, we find that the design space for HI is substantially enlarged and that the time scales can be substantially relaxed. This eliminates the assumptions on the nature of the bath in the one-dimension case which is required<sup>10</sup> to act very rapidly to prevent recrossing back to the original bright state. This in turn could then lead to increased dissipation on the bright state manifold and to the loss of HI efficiency.

The population accumulated on the bottom of the bright state can be recycled. Excited state absorption can transfer population to the dark state. This is of an additional advantage for utilizing the red part of the solar spectrum which otherwise will be dissipated to heat.

## HAMILTONIAN MODEL AND DYNAMICAL EVOLUTION OF THE SYSTEM DENSITY

It follows from the description above that there will be three relevant, important times for the evolution of the initial excited state: The first will be the very short period immediately after

excitation, where the vibrational wave packet exits its initial vertically excited state geometry and starts to evolve.

The second instance describes motion toward the crossing region, crossing and the avoidance of return to the bright state, and the third instance describes the long time relaxation dynamics in the dark or bright states.

The model represents a multimode molecular system coupled to a radiation field. The molecular system is subject to dissipative forces due to coupling to a primary bath. In turn the primary bath is subject to interactions with a secondary bath, and the total system + bath Hamiltonian is

$$\hat{H}_T = \hat{H}_S + \hat{H}_B + \hat{H}_{B''} + \hat{H}_{SB} + \hat{H}_{BB''} \quad (1)$$

where  $\hat{H}_S$  is the molecular Hamiltonian,  $\hat{H}_B$  the primary bath Hamiltonian,  $\hat{H}_{SB}$  the molecular bath coupling,  $\hat{H}_{B''}$  the secondary bath Hamiltonian, and  $\hat{H}_{BB''}$  is the primary/secondary bath coupling. The molecular system Hamiltonian is partitioned to the static part and interaction with the radiation.

$$\hat{H}_S = \begin{pmatrix} \hat{H}_g & 0 & 0 \\ 0 & \hat{H}_b & \hat{V}_{bd} \\ 0 & \hat{V}_{db} & \hat{H}_d \end{pmatrix} + \hat{H}_{EX} \quad (2)$$

where the operators are functions of the nuclear coordinates:  $\hat{H}_k = \sum_j^N (\hat{P}_j^2 / 2m_j) + (\hat{V}_k(\vec{r}))$  is the relevant  $N$ -mode vibrational Hamiltonian, and  $\hat{V}_k(\vec{r})$  is the ground (g), bright (b), or acceptor (dark) (d) potential and is a function of the  $N$  nuclear coordinates  $\vec{r}$ . Effectively we model two active molecular vibrational modes, and the remainder are put into the bath.

$\hat{V}_{bd}(\vec{r})$  represents the nonadiabatic coupling between the excited surfaces.

The excitation Hamiltonian is described by

$$\hat{H}_{EX} = \begin{pmatrix} 0 & \hat{\mu}_{gb} \epsilon(t) & 0 \\ \hat{\mu}_{bg} \epsilon^*(t) & 0 & \hat{\mu}_{bd} \epsilon(t) \\ 0 & \hat{\mu}_{db} \epsilon^*(t) & 0 \end{pmatrix} \quad (3)$$

where the transition dipole operator  $\hat{\mu}_{gb}$  is chosen to couple only the ground and the bright excited states and  $\epsilon(t)$  represents the time-dependent electromagnetic field. Another feature is an additional dipole coupling between the bright and dark excited states  $\hat{\mu}_{bd}$  for secondary pumping to increase the efficiency and reduce cooling requirements. To model the solar absorption in a time-dependent description we choose  $\epsilon(t)$  to be the Fourier transform of the solar spectrum. This results in a pulse duration of ~2.5 fs. For comparison we employ a Gaussian excitation pulse:  $\epsilon(t) = F_0 \exp[(-t^2 / 2\tau_0^2) + i\omega_0 t]$  where  $F_0$  is the light field intensity,  $\tau_0$  the temporal pulse width, and  $\omega_0$  the central frequency.

The potential forms used are summarized in Table 1. Figure 1 shows the system's potential landscape and a schematic view of the energetics.

The bath is described by a fully quantum formulation. The method employed is the stochastic surrogate Hamiltonian.<sup>11,12</sup> Briefly, the bath is divided into a primary part interacting with the system directly and a secondary bath which eliminates recurrence. The primary bath Hamiltonian is composed of a collection of two-level-systems.

$$\hat{H}_B = \hbar \sum_j \omega_j \hat{\sigma}_j^+ \hat{\sigma}_j^- \quad (4)$$

**Table 1. Potential Parameters: The Vibrational States Are Described in 2 Dimensions with Morse Potentials Where  $\bar{V}_{k,i}(r_1, r_2) = \sum_i D_{k,i} [1 - \exp(-\alpha_{k,i}(r_{k,i} - \bar{r}_{k,i}))]^2 + E_k$  Where  $k$  is the Surface Index,  $i$  the Vibrational Dimension Index, and  $\bar{r}_{k,i}$  the Position of the Potential Minimum for a Given ( $k, i$ )<sup>a</sup>**

$r_1$ :	values	units	$r_2$	values	units
$D_{g1}$	4.75	eV	$D_{g2}$	4.55	eV
$\alpha_{g1}$	0.75	bohr <sup>-1</sup>	$\alpha_{g2}$	0.5	bohr <sup>-1</sup>
$\bar{r}_{g1}$	1.4	bohr	$\bar{r}_{g2}$	1.75	bohr
$E_g$	0.	eV	$E_g$	0.	eV
$D_{b1}$	3.275	eV	$D_{b2}$	3.725	eV
$\alpha_{b1}$	0.9	bohr <sup>-1</sup>	$\alpha_{b2}$	1.5	bohr <sup>-1</sup>
$\bar{r}_{b1}$	1.45	bohr	$\bar{r}_{b2}$	1.2	bohr
$E_b$	1.85	eV	$E_b$	0	eV
$D_{d1}$	2.725	eV	$D_{d2}$	3.725	eV
$\alpha_{d1}$	0.4	bohr <sup>-1</sup>	$\alpha_{d2}$	1.1	bohr <sup>-1</sup>
$\bar{r}_{d1}$	2.75	bohr	$\bar{r}_{d2}$	1.14	bohr
$E_d$	2.1	eV	$E_d$	0.0	eV
$V_r$	0.17	eV	$V_c$	0.	eV
$\beta_j$	1.2	bohr <sup>-1</sup>	$\gamma_c$	0.5	bohr <sup>-2</sup>

<sup>a</sup>For  $k$ , we use g, b, and d subscripts describing the ground, bright, and dark acceptor states. The nonadiabatic coupling has an exponential decay in  $r_2$ , the strong vibrational mode dimension, and a Gaussian centered along the seam in  $r_1$ , the soft vibrational mode dimension:  $\bar{V}_{bd}(r_1, r_2) = V_r \cdot \exp(-\beta_j(r_1 - \bar{r}_1)) \cdot \exp(-\gamma_c(r_2 - \bar{r}_2)^2)$ , where  $\bar{r}_2$  is located at the seam between  $V_b$  and  $V_d$ .

The energies  $\omega_j$  represent the spectrum of the bath, and  $\hat{\sigma}_{\pm}$  are bath excitation/de-excitation operators. The system–bath interaction  $\hat{H}_{SB}$  can be chosen to represent different physical processes.<sup>11–14</sup> Specifically (following ref 11) we choose an interaction leading to vibrational relaxation

$$\hat{H}_{SB} = \hbar f(\hat{\mathbf{R}}_s) \otimes \sum_j^N \lambda_j (\hat{\sigma}_j^\dagger + \hat{\sigma}_j) \quad (5)$$

where  $f(\hat{\mathbf{R}}_s)$  is a dimensionless function of the system nuclear coordinates  $\hat{\mathbf{R}}_s$  and  $\lambda_j$  is the system–bath coupling frequency of bath mode  $j$ . When the system–bath coupling is characterized by a spectral density  $J(\omega) = \sum_j |\lambda_j|^2 \delta(\omega - \omega_j)$  then  $\lambda_j = (J(\omega_j)/\rho_j)^{1/2}$ , and  $\rho_j = (\omega_{j+1} - \omega_j)^{-1}$  is the density of bath modes.

The secondary bath is also composed of noninteracting two-level systems (TLSs) at temperature  $T$  with the same frequency spectrum as the primary bath. At random times the states of primary and secondary bath modes of the same frequency are swapped at a rate  $\Gamma_j^{11–13,15}$  (cf. Appendix). The bath employed was chosen to generate a vibrational relaxation time of approximately  $T_1 = 1$  ps for the stiff mode and 5 ps for the soft mode in the different potentials. The swapping procedure permits description of both dephasing and energy relaxation. The final results are obtained by averaging over the stochastic realizations. The swap makes the bath effectively infinite. Each swap operation eliminates the quantum correlation between the bath mode swapped and system and other bath modes. This loss of system–bath correlation leads to dephasing.

The stochastic surrogate Hamiltonian approach is a fully quantum treatment of system–bath dynamics. The method is not Markov constrained and is based on a wave function construction. The system and bath are initially correlated since the initial state is the combined thermal state generated from the coupled system–bath Hamiltonian by propagating in imaginary time<sup>16</sup> until the correlated ground state is obtained. The transport properties of the surrogate Hamiltonian are

consistent with the second law of thermodynamics.<sup>17</sup> Additional entanglement is generated by the dynamics. Convergence of the model is obtained by increasing the number of bath modes and the number of stochastic realizations. The parameters of the model are summarized in Tables 1 and 2.

**Table 2. Propagation Parameters: The Initial State Is the Vibrational Ground State of  $\hat{V}_g(r)$  Obtained by Propagation in Imaginary Time<sup>26a</sup>**

pulse parameters	typical values	units
$\omega_0$	20600	cm <sup>-1</sup>
$\tau_0$	6.0	fs
$F_0$	0.2	eV
grid parameters	typical values	units
grid spacing, $\Delta r$	0.03125	bohr
number of grid points, $N_r$	128	
time steps, $\Delta t$	0.5	fs
order of Chebychev polynomials	128	
reduced mass $m$	16	amu
bath parameters	typical values	units
number of bath modes	12	
cutoff frequency $\omega_c$	1.6	eV
system–bath coupling range $\zeta$	1.945	bohr <sup>-1</sup>
swap rate $\Gamma_j/\lambda_j$	1.05	

<sup>a</sup>The system wave function is represented on a Fourier grid of  $N_r$  points.<sup>27</sup> Propagation is carried out by the Chebychev method.<sup>16</sup> The system–bath coupling function is chosen to be linear  $f(r) = \zeta(r - r_k)$  (eq 5). The spectral density  $J(\omega)$  is chosen to be Ohmic with a cutoff frequency of  $\omega_c$ .

## OPTIMIZED SYSTEM DESIGN

The following design principles can be used to optimize the process:

1. Absorption spectra: In the energy band of possible solar capture, the absorption spectrum should reasonably match the solar spectrum (cf. Figure 2).
2. Nonadiabatic transfer: We position the bright/dark crossing seam higher than the energy for vertical excitation from the ground state, to ensure that the reverse process from dark to bright is improbable. This will capture the high energy part of the solar spectrum in the dark (acceptor) state, thus acting as an effective energy rectifier.
3. Efficient transfer from the bright state to the dark state, requiring a vibrational mode with a strong projection of the motion directed toward the crossing seam, even in multiple dimensions.
4. Stabilization by motion along a soft vibrational mode followed by energy dissipation into the environment.
5. Secondary solar capture by employing the red part of the solar spectrum to transfer population from the bottom of the bright state to the dark state.

Figure 2 shows the calculated absorption spectrum of the model system superimposed on the solar spectrum. The chosen molecular spectrum successfully overlaps much of the high energy part of the solar spectrum. Such a spectrum can be generated by designing a molecule with high vibrational frequency and large zero-point displacement in the bright electronic state and a soft vibrational mode in the ground state. Additional performance can be obtained by photoexciting from the bright to the dark states utilizing the red portion of the solar

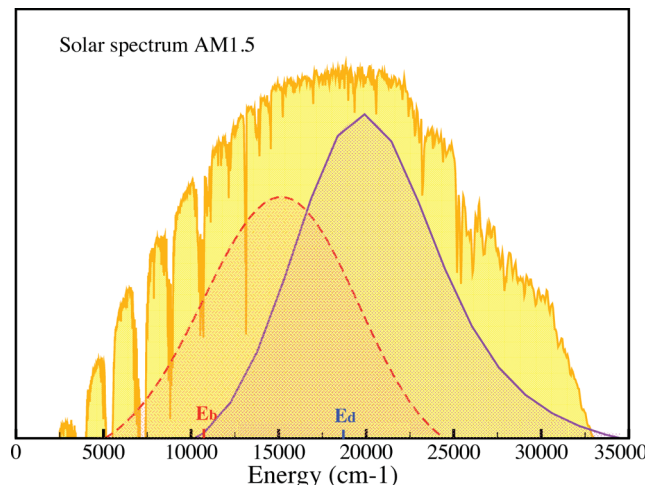


**Figure 2.** Standard solar spectrum and the absorption spectrum of the molecular model. The solid line represents the ground state absorption spectra calculated directly by solving the TDSE. The initial state was the equilibrium state on the ground potential. The energy absorbed from a weak pulse with a specified carrier frequency was used to compose the spectrum by repeating the calculation with different carrier frequencies. The dashed line represents the absorption spectrum of the bright to dark acceptor state. The same procedure was used with the initial wave function residing on the bright state potential. The collection energy points (from Figure 1)  $E_d$  and  $E_b$  are indicated.

spectrum. The absorption spectrum of this second transition is indicated in Figure 2.

**Efficiency of Design.** A solar converter model is an example of a device converting heat to work. Such a device is limited by the Carnot efficiency  $\eta_c \leq 1 - T_c/T_h$ . The solar radiation is characterized by a temperature of  $T_h = 5600$  K, and entropy is ejected to a cold bath of temperature  $T_c = 300$  K. The maximum possible thermodynamic efficiency is  $\eta_c \sim 95\%$ . A more realistic estimate incorporates the finite time dynamics with the trade-off between efficiency and power.<sup>18–20</sup>

Specifically, the efficiency of the design can be estimated by first calculating the average photon energy in the solar spectrum

$$E_{\text{sol}} = \int_0^{\infty} EP_{\text{sol}}(E) dE \quad (6)$$

where  $P_{\text{sol}}(E)$  is the normalized solar spectrum in inverse energy units. If only the dark state energy  $E_d$  is harvested then the energy that can be obtained is

$$\bar{E}_d = E_d \int_{E_d}^{\infty} P_{\text{sol}}(E) P_{\text{gb}}^a(E) P_{\text{bd}}^t(E) dE \quad (7)$$

where  $P_{\text{gb}}^a(E)$  is the absorption spectrum probability. It is determined by the absorption cross section and the concentration of absorbers. This probability can be saturated  $P_{\text{gb}}^a(E) = 1$  for the region around the maximum.  $P_{\text{bd}}^t(E)$  is the branching probability between the bright and dark state. The branching probability  $P_{\text{bd}}^t(E)$  is estimated by employing a series of Gaussian pulses of width  $\tau = 40$  fs with the carrier frequency  $\hbar\omega_0 = E$  for different energies  $E$ :  $\epsilon(t) = (F_0 e^{i\omega_0 t}) (e^{(-t^2/2\tau^2)})$  where the intensity  $F_0$  is in the weak field regime. We then normalize the wave function on the bright state and complete the propagation until the branching probability is obtained for each energy.

The energetic efficiency of the dark state becomes

$$\eta_d = \frac{\bar{E}_d}{E_{\text{sol}}} \quad (8)$$

Equation 8 is restricted by the Shockley–Queisser limit<sup>21</sup> which is obtained if  $P_{\text{bd}}^t(E) = 1$  and the absorption spectra is saturated  $P_{\text{gb}}^a(E) = 1$ . For the present model the dark state only efficiency is  $\eta_d = 0.226$  when  $P_{\text{gb}}^a(E) = 1$ . This can be compared to the efficiency when  $P_{\text{gb}}^a(E)$  is normalized to the maximum absorption energy leading to  $\eta_d = 0.101$ .

To increase the efficiency beyond a single energy harvesting point (cf. Figure 1), one option is to extract also the energy stored at the bottom of the bright state. Then additional energy is obtained

$$\bar{E}_b = E_b \int_{E_b}^{\infty} P_{\text{sol}}(E) P_{\text{gb}}^a(E) (1 - P_{\text{bd}}^t(E)) dE \quad (9)$$

where  $E_b$  is the energy of the bottom of the bright state well.

The efficiency of the device, if collection occurs from both bright and dark states, is

$$\eta_{d+b} = \frac{\bar{E}_d + \bar{E}_b}{E_{\text{sol}}} \quad (10)$$

For this model the total efficiency is  $\eta_{d+b} = 0.36$  when the absorption spectrum  $P_{\text{gb}}^a(E)$  is saturated. For the normalized case when only the maximum absorption frequency is saturated  $\eta_{d+b} = 0.18$ . The drawback of this design is that it requires two extraction leads, one connected to the bottom of the dark state and one connected to the bottom of the bright state. An improved design option is to repump the energy from the bottom of the bright state to the dark state using the unemployed red part of the solar spectrum. The extra amount of energy obtained in this route becomes

$$\bar{E}_{b'} = E_d \int_{E_b}^{\infty} P_{\text{sol}}(E) P_{\text{gb}}^a(E) (1 - P_{\text{bd}}^t(E)) dE \int_{E_d - E_b}^{\infty} P_{\text{sol}}(E') P_{\text{bd}}^a(E') dE' \quad (11)$$

which leads to the efficiency

$$\eta_{d+b'} = \frac{\bar{E}_d + \bar{E}_{b'}}{E_{\text{sol}}} \quad (12)$$

with the advantage that the energy extraction is carried out from one lead at the bottom of the dark state. The total efficiency  $\eta_{d+b'} = 0.58$  for saturated  $P_{\text{gb}}^a(E)$  and  $\eta_{d+b'} = 0.128$  for saturation only at the maximum.

## RESULTS

The operation of the molecular solar energy converter can be followed sequentially by solving the time-dependent Schrödinger

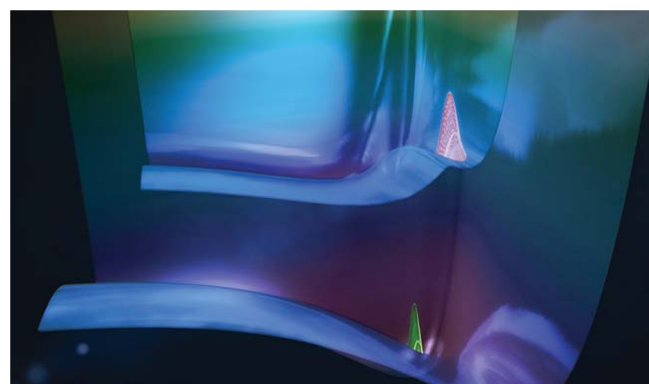


**Figure 3.** Split wave function on the ground and bright state during the excitation pulse.

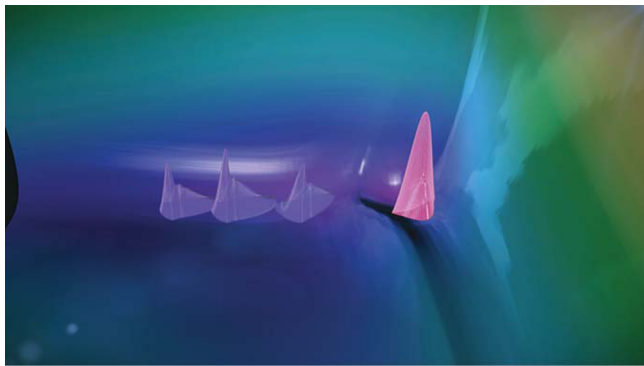


**Figure 4.** First encounter: The bright and dark components of the photoexcited wave function near the crossing seam.

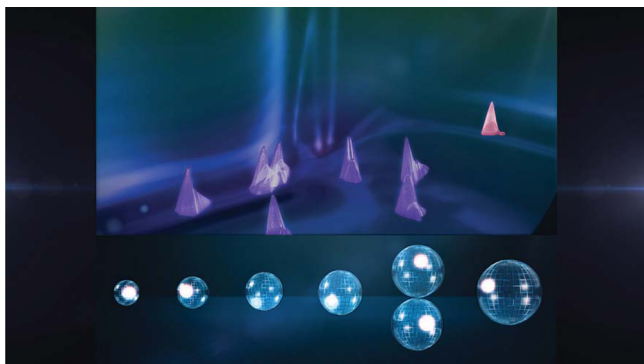


**Figure 5.** Snapshot of the combined system–bath system. Top: the probability density of the system superimposed on the excited state potential. Bottom: The reduced state of the spin bath in the process of a swap. The reduced state of each bath mode is represented on a Bloch sphere. The radius of the sphere is proportional to the frequency of the mode. The internal state of the spin is indicated as a dot.

equation:  $i\hbar(\partial\Psi/\partial t) = \hat{H}\Psi$  with the Hamiltonian of eq 1. The starting point is an ultrashort pulse with the spectral properties of the solar spectrum. In a weak field this pulse transfers population from the ground to the bright state which is equivalent to

population transfer induced by weak CW solar radiation. The initial state  $\Psi(t=0)$  is in equilibrium on the ground surface. The calculations follow the procedures of the Stochastic Surrogate Hamiltonian.<sup>11</sup>

Figure 3 shows the split wave function on the ground and excited bright state during the excitation.

Once population reaches the bright state it evolves dynamically due to the forces induced by the excited state potentials. When the wave function reaches the crossing seam with the dark state, population is partially transferred. This event is captured by Figure 4. On this time scale the system–bath dynamics is insignificant. Figure 5 is a snapshot of the system–bath state where the surrogate bath state is represented by the position of the local spin on the Bloch sphere. A swap operation exchanging one of the primary bath spins with the secondary bath is also visible. Eventually, the bath modifies the dynamics, stabilizing the product. The influence of the system–bath dynamics can be observed in Figure 6 which compares the dynamics with and without the bath. Without the bath the dynamics is reversible. Population flows periodically between the bright and dark state. The bath, by dissipating energy, moves the density below the crossing seam energy thus stabilizing the products. This is the origin of the rectifying effect: a unidirectional flow of energy to the dark state.

The whole excitation stabilization event is shown in Figure 7, showing the dynamics of the projected molecular state (after tracing over the bath). Initially, the bright state molecular density is localized in the Franck–Condon position. The initial motion is in the direction of the fast mode toward the crossing seam to the dark acceptor state. Subsequent dynamics in the soft mode effectively switches off the bright to dark transition. Finally, energy relaxation to the bath modes localizes the molecular density in the bottoms of the bright and dark states. As a result the high energy part of the solar spectrum is captured in the acceptor dark state and the lower portion in the bases of the bright state. Further examination of the dynamics shows that the localization due to relaxation is faster on the bright state. Optimizing the yield requires a balance between the system's reversible Hamiltonian-generated dynamics and the dissipative forces. The sweet spot is related to the general

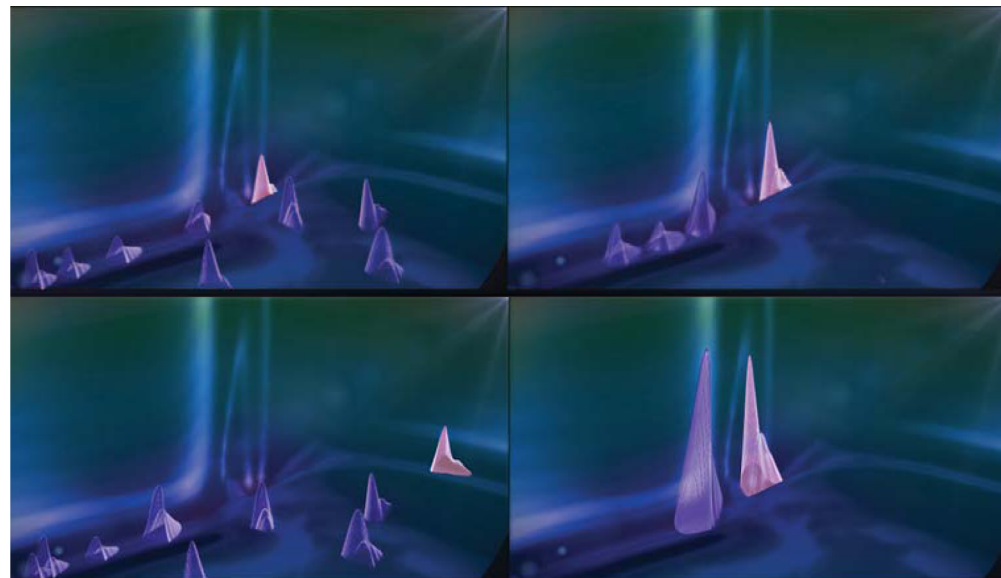


**Figure 6.** Dynamics on the excited state with the surrogate bath on the right and without the bath on the left. The snapshots of the wave function are shown for 2 ps and 10 ps. At the final time the density of the combined system–bath is localized in the bright and dark potential wells.

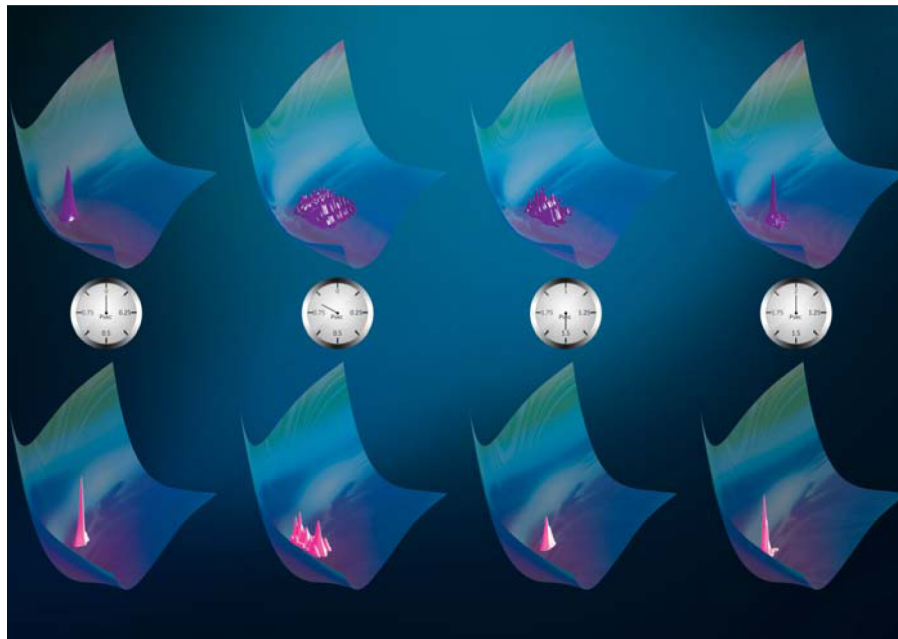


**Figure 7.** Dynamics of the projected molecular state on the bright bottom (pink) and acceptor top (maroon) electronic states superimposed on the excited adiabatic potential energy surfaces. The left panel shows the molecular state immediately after the first excitation pulse. The next panel shows the molecular state after 800 fs and the next panel 1500 fs. The right panel shows the wave function concentration after 2000 fs.

turnover effect.<sup>22,23</sup> Underdamping will not generate a rectifying effect. Overdamping will generate a Zeno-like effect and inhibit the transport. There are indications of a similar balance in natural photosynthesis.<sup>24</sup>

The simulation can be continued by applying a series of solar spectral pulses. If the time delay between pulses is sufficient the bath relaxation eliminates all phase information shared between the pulses. This means that a series of incoherent short and weak pulses is equivalent to CW solar excitation.<sup>25</sup> For a design where the power output is extracted from the bottom of the dark state, and with no repumping of the bright state, a simulation including a single pulse is adequate.

For the enhanced design where, in addition to the ground state absorption to the bright state, the bright to dark absorption is also utilized to harvest the red part of the solar spectrum, the simulation is continued by applying a series of pulses. Figure 8 shows the population accumulated on the bright and

dark states during a series of short pulses, each of which is generated from the Fourier transform of the solar spectrum. All these pulses are in the weak field regime. Initially, the radiation-induced population transfer occurs exclusively from the ground to the bright state. After many such pulses population accumulates on the bright state causing an additional population transfer from the bright to the dark state. Accumulating many such pulses causes the population on the dark state to dominate.

To complete the photocycle a mechanism to harvest the dark state has to be specified. Typically, such a device has a longer time scale than the fast absorption and stabilization which terminates in approximately  $\sim 2.5$  ps. The energy extraction has to be accompanied by restoring equilibrium population on the ground electronic surface.

## CONCLUSIONS

We have explored a novel design of a molecular acceptor for solar energy. Dissipation, which is typically a loss term, is employed to generate a rectifying action, stabilizing the energy caches. The design principles include a fast mode utilized to remove density from the FC configuration and soft modes combined with a dissipative bath to stabilize the dark state energy cache. This design allows minimization of the energy loss to dissipation.

The population trapped in the bright state is not wasted. By designing the molecule properly, the red, unutilized part of the solar spectra is employed to get additional population in the dark energy cache. This mechanism has the additional benefit of reducing the cooling requirements of the device.

The maximum efficiency of the model is obtained when the absorption spectrum is saturated. In the present model it reaches 22% for harvesting from the bottom of the dark state, when only the absorption from the ground to the bright state is operating. The efficiency increases to 36% if the energy is harvested from both the bright and dark states. The efficiency can reach 58% if the transition from the bright to the dark state is included.

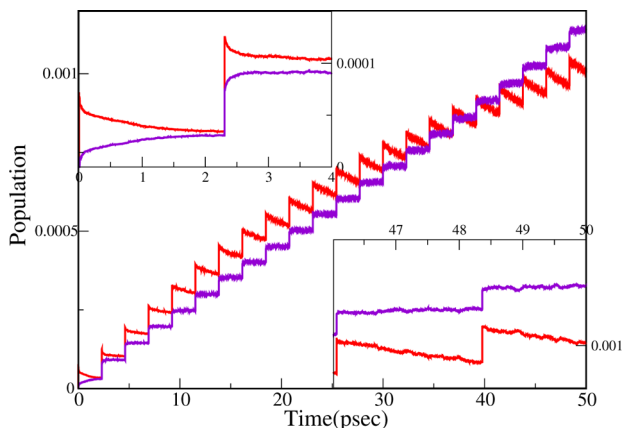


**Figure 8.** Population on the bright state (red) and dark state (blue) as a function of time after a series of incoherent pulses modeling the solar illumination. The insert zooms in on the first two excitation events (left) and on the last two excitations (right).

## APPENDIX: SWAP OPERATION

A central operation in the stochastic surrogate Hamiltonian is the swap: replacing one spin component of the bath with another. An important technical issue is how to perform this operation within a global wave function description of the system and primary bath. This implementation is illustrated by a simple example.

The implementation of the swap operation depends on the method of representation. Consider the single spin (qubit) general wave function

$$|\psi\rangle = \alpha|0\rangle + \beta|1\rangle \quad (13)$$

where  $\alpha^2 + \beta^2 = 1$ . A different representation employs an exponential form

$$|\psi\rangle = \frac{1}{Z}(e^b|0\rangle + e^{-b}|1\rangle) \quad (14)$$

where  $b$  is complex. The relation between the two representations is  $e^{2b} = \alpha/\beta$  when we choose the convention that the total phase is zero. The normalization becomes  $Z^2 = 2 \cosh(b + b^*)$ .

For a multispin case the swap operation is carried out by switching between two representations: For example for three spins the wave function can be represented as

$$\begin{aligned} |\psi\rangle &= \lambda_1|000\rangle + \lambda_2|001\rangle + \lambda_3|010\rangle + \lambda_4|011\rangle + \lambda_5|100\rangle + \lambda_6|101\rangle \\ &+ \lambda_7|110\rangle + \lambda_8|111\rangle = \frac{1}{Z}(e^{a_1}|000\rangle + e^{a_2}|001\rangle + e^{a_3}|010\rangle + e^{a_4}|011\rangle \\ &+ |100\rangle e^{a_5} + |101\rangle e^{a_6} + |110\rangle e^{a_7} + |111\rangle e^{a_8}) \end{aligned} \quad (15)$$

We choose a convention that the total phase is zero. In addition we impose a similar relation on the real part:  $\sum_j a_j = 0$ . This leads to the normalization condition:  $Z^2 = \sum_j e^{a_j + a_j^*}$ . An alternative conditional coding scheme based on a branching tree facilitates the swap operation.

$$\begin{aligned} a_1 &= \alpha + \alpha\alpha + \alpha\alpha\alpha \\ a_2 &= \alpha + \alpha\alpha + \alpha\alpha\beta \\ a_3 &= \alpha + \alpha\beta + \alpha\beta\alpha \\ a_4 &= \alpha + \alpha\beta + \alpha\beta\beta \\ a_5 &= \beta + \beta\alpha + \beta\alpha\alpha \\ a_6 &= \beta + \beta\alpha + \beta\alpha\beta \\ a_7 &= \beta + \beta\beta + \beta\beta\alpha \\ a_8 &= \beta + \beta\beta + \beta\beta\beta \end{aligned} \quad (16)$$

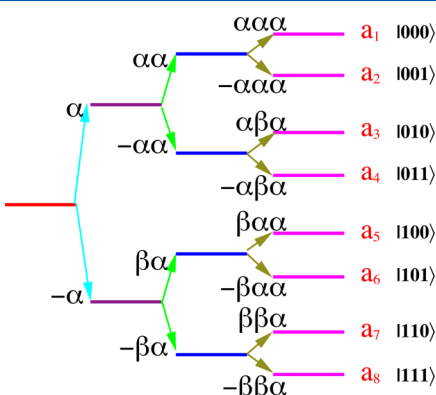


**Figure 9.** Coding scheme of the spin bath. On the right, the amplitude code  $\lambda_j = e^{a_j}$  in the product base. On the left, the branching code.

With this coding we have eight  $\{a_j\}$  coefficients which are constrained to sum to zero. We have 14 branching coefficients. We impose  $\alpha = -\beta$ ,  $\alpha\alpha = -\alpha\beta$ ,  $\beta\alpha = -\beta\beta$ ,  $\alpha\alpha\alpha = -\alpha\alpha\beta$ ,  $\alpha\beta\alpha = -\alpha\beta\beta$ ,  $\beta\alpha\alpha = -\beta\alpha\beta$ , and  $\beta\beta\alpha = -\beta\beta\beta$ . This means that we have seven independent coefficients in each set (cf. Figure 9).

The relation between the parameters can be written as

$$\begin{pmatrix} a_1 \\ a_2 \\ a_3 \\ a_4 \\ a_5 \\ a_6 \\ a_7 \\ a_8 \end{pmatrix} = \begin{pmatrix} 1 & 1 & 0 & 1 & 0 & 0 & 0 & 0 \\ 1 & 1 & 0 & -1 & 0 & 0 & 0 & 0 \\ 1 & -1 & 0 & 0 & 1 & 0 & 0 & 0 \\ 1 & -1 & 0 & 0 & -1 & 0 & 0 & 0 \\ -1 & 0 & 1 & 0 & 0 & 1 & 0 & 0 \\ -1 & 0 & 1 & 0 & 0 & -1 & 0 & 0 \\ -1 & 0 & -1 & 0 & 0 & 0 & 1 & 0 \\ -1 & 0 & -1 & 0 & 0 & 0 & -1 & 0 \end{pmatrix} \begin{pmatrix} \alpha \\ \alpha\alpha \\ \beta\alpha \\ \alpha\alpha\alpha \\ \alpha\beta\alpha \\ \beta\alpha\alpha \\ \beta\beta\alpha \\ 0 \end{pmatrix} \quad (17)$$

The inverse relation becomes

$$\begin{pmatrix} \alpha \\ \alpha\alpha \\ \beta\alpha \\ \alpha\alpha\alpha \\ \alpha\beta\alpha \\ \beta\alpha\alpha \\ \beta\beta\alpha \\ 0 \end{pmatrix} = \begin{pmatrix} \frac{1}{8} & \frac{1}{8} & \frac{1}{8} & \frac{1}{8} & -\frac{1}{8} & -\frac{1}{8} & -\frac{1}{8} & -\frac{1}{8} \\ \frac{1}{4} & \frac{1}{4} & -\frac{1}{4} & -\frac{1}{4} & 0 & 0 & 0 & 0 \\ 0 & 0 & 0 & 0 & \frac{1}{4} & \frac{1}{4} & -\frac{1}{4} & -\frac{1}{4} \\ \frac{1}{2} & -\frac{1}{2} & 0 & 0 & 0 & 0 & 0 & 0 \\ 0 & 0 & \frac{1}{2} & -\frac{1}{2} & 0 & 0 & 0 & 0 \\ 0 & 0 & 0 & 0 & \frac{1}{2} & -\frac{1}{2} & 0 & 0 \\ 0 & 0 & 0 & 0 & 0 & 0 & \frac{1}{2} & -\frac{1}{2} \\ 1 & 1 & 1 & 1 & 1 & 1 & 1 & 1 \end{pmatrix} \begin{pmatrix} a_1 \\ a_2 \\ a_3 \\ a_4 \\ a_5 \\ a_6 \\ a_7 \\ a_8 \end{pmatrix} \quad (18)$$

These equations show that there is a one to one linear relation between the two sets of wave function parameters.

The swap operation is demonstrated on the outer branches of the spin tree.

- From the computational set of coefficients  $\{\lambda_j\}$  eq 15 calculate the set  $\{a_j\}$ .
- From  $\{a_j\}$  calculate the branching set coefficients  $\alpha, \alpha\alpha, \beta\alpha, \alpha\alpha\alpha, \dots$
- Change all the coefficients  $\alpha\alpha\alpha = \alpha\beta\alpha = \beta\alpha\alpha = \beta\beta\alpha = b$  to the value  $b$  of a swapped spin.
- From the branching set recalculate the set  $\{a_j\}$  and renormalize.
- Recalculate  $\{\lambda\}$ .

The result of the swap operation is a tensor product state between the swapped spin and the rest

$$|\Psi\rangle = (\lambda_1|00\rangle + \lambda_2|01\rangle + \lambda_3|10\rangle + \lambda_4|11\rangle) \otimes (\lambda_5|0\rangle + \lambda_6|1\rangle)$$

and

$$\lambda_5/\lambda_6 = e^{2b}$$

## ASSOCIATED CONTENT

### S Supporting Information

Movie. An animation describing the method of simulation of solar capture solving the time dependent Schrödinger equation for system and bath is presented as a movie in the supplement information. This material is available free of charge via the Internet at <http://pubs.acs.org>.

## AUTHOR INFORMATION

### Corresponding Authors

\*E-mail: gkatz@afmilk.co.il

\*E-mail: ratner@chem.northwestern.edu

\*E-mail: ronnie@fl.huji.ac.il.

## Notes

The authors declare no competing financial interest.

## ACKNOWLEDGMENTS

We thank the Israel Science Foundation, the Chemistry Divisions of the National Science foundation, and the ONR for partial support. This work was supported as part of the ANSER Center, an Energy Frontier Research Center funded by the U.S. Department of Energy, Office of Science, Office of Basic Energy Sciences, under Award Number DE-SC0001059.

## REFERENCES

- (1) Kurtz, S. R.; Olson, J.; Faine, P. The difference between standard and average efficiencies of multijunction compared with single-junction concentrator cells. *Sol. Cells* **1991**, *30*, 501–513.
- (2) Philipps, S.; Peharz, G.; Hoheisel, R.; Hornung, T.; Al-Abbadia, N.; Dimroth, F.; Bett, A. Energy harvesting efficiency of III-V triple-junction concentrator solar cells under realistic spectral conditions. *Sol. Energy Mater. Sol. Cells* **2010**, *94*, 869–877.
- (3) Beard, M. C.; Ellingson, R. J. Multiple exciton generation in semiconductor nanocrystals: Toward efficient solar energy conversion. *Laser Photonics Rev.* **2008**, *2*, 377–399.
- (4) Kasha, M. Characterization of electronic transitions in complex molecules. *Discuss. Faraday Soc.* **1950**, *9*, 14–19.
- (5) McNaught, A. D.; Wilkinson, A. *IUPAC Compendium of chemical terminology*; Blackwell Science: Cambridge, MA, 2000
- (6) Klan, P.; Witz, J. *Photochemistry of Organic Compounds: From Concepts to Practice*; Wiley: New York, 1994.
- (7) Guo, X.-L.; Dong, Z.-C.; Trifonov, A.; Miki, K.; Kimura, K.; Mashiko, S. STM-induced light emission from the surface of H<sub>2</sub>TBP porphyrin/PFP porphyrin/Cu(1 0 0). *Appl. Surf. Sci.* **2005**, *241*, 28–32.
- (8) Boudreaux, D.; Williams, F.; Nozik, A. Hot Carrier Injection at Semiconductor-Electrolyte Junctions. *J. Appl. Phys.* **1980**, *51*, 2158–2163.
- (9) Yang, S. Y.; Qian, L.; Teng, F.; Xu, Z.; Xu, X. R. Alternating-current electroluminescence from an organic heterojunction sandwiched between two amorphous SiO<sub>2</sub> layers. *J. Appl. Phys.* **2005**, *97*, 126101.
- (10) Katz, G.; Ratner, M. A.; Kosloff, R. Hot Injection Dynamics: Design Mechanisms and Ideas. *J. Phys. Chem. A* **2010**, *115*, 5833–5837.
- (11) Katz, G.; Gelman, D.; Ratner, M. A.; Kosloff, R. Stochastic surrogate Hamiltonian. *J. Chem. Phys.* **2008**, *129*, 034108.
- (12) Katz, G.; Ratner, M. A.; Kosloff, R. Control by decoherence: weak field control of an excited state objective. *New J. Phys.* **2010**, *12*, 015003.
- (13) Koch, C. P.; Klüner, T.; Kosloff, R. A complete quantum description of an ultrafast pump-probe charge transfer event in condensed phase. *J. Chem. Phys.* **2002**, *116*, 7983–7996.
- (14) Koch, C. P.; Klüner, T.; Freund, H.-J.; Kosloff, R. Femtosecond Photodesorption of Small Molecules from Surfaces: A Theoretical Investigation from First Principles. *Phys. Rev. Lett.* **2003**, *90*, 117601.
- (15) Koch, C. P.; Klüner, T.; Freund, H.-J.; Kosloff, R. Surrogate Hamiltonian study of electronic relaxation in the femtosecond laser induced desorption of NO/NiO(100). *J. Chem. Phys.* **2003**, *119*, 1750–1765.
- (16) Tal-Ezer, H.; Kosloff, R. An accurate and efficient scheme for propagating the time dependent Schrödinger equation. *J. Chem. Phys.* **1984**, *81*, 3967–3971.
- (17) Levy, A.; Kosloff, R. The local approach to quantum transport may violate the second law of thermodynamics. *Europhys. Lett.* **2014**, *107*, 20004.
- (18) Salamon, P.; Nulton, J.; Siragusa, G.; Andersen, T. R.; Limon, A. Principles of Control Thermodynamics. *Energy* **2001**, *26*, 307–319.
- (19) Esposito, M.; Kawai, R.; Lindenberg, K.; Van den Broeck, C. Efficiency at maximum power of low dissipation Carnot engines. *Phys. Rev. Lett.* **2010**, *105*, 150603.
- (20) Kosloff, R. Quantum Thermodynamics: A Dynamical Viewpoint. *Entropy* **2013**, *15*, 2100–2128.
- (21) Shockley, W.; Queisser, H. J. Detailed Balance Limit of Efficiency of *p-n* Junction Solar Cells. *J. Appl. Phys.* **1961**, *32*, 510–519.
- (22) Ashkenazi, G.; Kosloff, R.; Ratner, M. A. Photoexcited Electron Transfer: Short-Time Dynamics and Turnover Control by Dephasing, Relaxation, and Mixing. *J. Am. Chem. Soc.* **1999**, *121*, 3386–3395.
- (23) Kosloff, R.; Ratner, M. A. Rate Constant Turnovers: Energy Spacings and Mixings. *J. Phys. Chem. B* **2002**, *106*, 8479–8483.
- (24) Mohseni, M.; Shabani, A.; Lloyd, S.; Omar, Y.; Rabitz, H. Geometrical effects on energy transfer in disordered open quantum systems. *J. Chem. Phys.* **2013**, *138*, 204309.
- (25) Han, A. C.; Shapiro, M.; Brumer, P. Nature of Quantum States Created by One Photon Absorption: Pulsed Coherent vs Pulsed Incoherent Light. *J. Phys. Chem. A* **2013**, *117*, 8199–8204.
- (26) Kosloff, R.; Tal Ezer, H. A Direct Relaxation Method for Calculating Eigenfunctions and Eigenvalues of the Schrödinger Equation On a Grid. *Chem. Phys. Lett.* **1986**, *127*, 223–230.
- (27) Kosloff, R. Time-dependent quantum-mechanical methods for molecular dynamics. *J. Phys. Chem.* **1988**, *92*, 2087–2100.